# DABCO-Metalloporphyrin Binding: Ternary Complexes, Host-Guest Chemistry, and the Measurement of $\pi$-$\pi$ Interactions

**Christopher A. Hunter, M. Nafees Meah, and Jeremy K. M. Sanders***

*Contribution from the Cambridge Centre for Molecular Recognition, University Chemical Laboratory, Lensfield Road, Cambridge CB2 1EW, U.K.* *Received October 31, 1989*

**Abstract:** Transient ternary complexes of the general form metalloporphyrin-DABCO-metalloporphyrin are described and characterized by NMR spectroscopy: the protons of DABCO (1,4-diazobicyclo[2.2.2]octane) molecules sandwiched between two diamagnetic metalloporphyrins resonate around -5 ppm. The same structural motif is shown to occur when DABCO binds within the cavity of cofacial metalloporphyrin dimers. The kinetics and thermodynamics of intracavity binding were measured by electronic and NMR spectroscopy and lead to an estimate of 48 ± 10 kJ mol$^{-1}$ (11.5 ± 2.4 kcal mol$^{-1}$) for the enthalpy of the $\pi$-$\pi$ interaction between two zinc porphyrin moieties. The mechanism of ligand exchange and isomer interconversion for one of the porphyrin dimers has also been elucidated.

If we are to develop effective synthetic models of complex systems such as enzymes, then we need an understanding of how intra- and intermolecular interactions arise and how they dictate the conformations adopted by flexible supramolecules. To this end we have been studying the properties of flexible macrocyclic porphyrin dimers.[1,2] In this paper, we describe the remarkably subtle host-guest chemistry of the cofacial dimers, $Zn_2$**1** and $Zn_2$**2**, and show how the kinetics and thermodynamics of binding allow us to estimate the strength of the $\pi$-$\pi$ interaction between the porphyrin moieties. In the following paper,[3] we extend this approach to more flexible porphyrin dimers that can accommodate large ligands within their cavities. In a related paper,[4] we present a simple electrostatic model which explains the geometry of the observed $\pi$-$\pi$ interactions, generalizes the theoretical framework for understanding intermolecular $\pi$-$\pi$ interactions, and proposes a series of rules for predicting when such interactions will occur.

A strong attractive interaction between the two porphyrin moieties in dimers **1** and **2** controls the geometry adopted by these systems.[5] Metallation with zinc increases the magnitude of the interaction, while coordination of the zinc by a ligand such as pyridine reduces it.[6] UV-visible spectra show that there is a strong electronic interaction between the excited states of the $\pi$-systems, while the ground state electronic wave functions of the individual porphyrin moieties are essentially unperturbed in the dimer.[7] This electronic interaction is therefore not responsible for the attraction between the porphyrins.

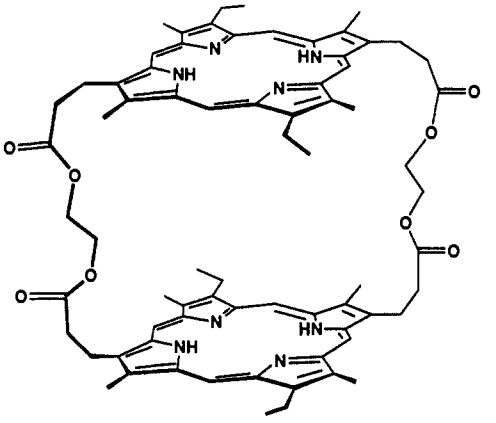

**1**

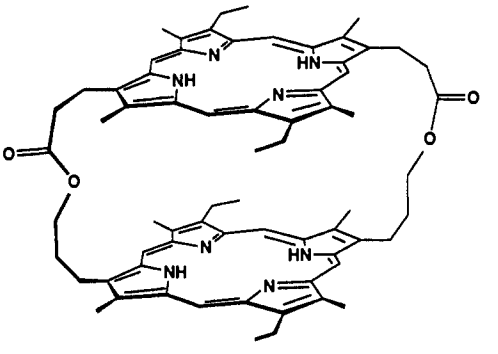

**2**

We describe here the binding of dimers $Zn_2$**1** and $Zn_2$**2** and of the corresponding monomer **Zn3**, to DABCO, **4**. This rigid bifunctional ligand binds inside the cavity to form a 1:1 complex with both dimers, even in the presence of a vast excess of the ligand (Figure 1). By using UV-visible absorption and $^1$H NMR spectroscopy we have elucidated the geometry of the complexes and the thermodynamic and kinetic parameters which control the reactions.

## Experimental Section

The porphyrins were synthesised as described previously.[5]

UV-visible absorption spectra were recorded in 1 cm × 1 cm cuvettes on a Pye Unicam PU 8800 spectrometer which had a variable temperature facility. All measurements were made on dichloromethane solutions, $10^{-7}$-$10^{-6}$ M in porphyrin. The apparatus was initially rigorously cleaned and dried, and the dichloromethane was distilled from calcium hydride.

(1) For studies of intermolecular interactions in rigid systems, see: (a) Tabushi, I.; Kugimiya, S.-I.; Kinnaird, M. G.; Sasaki, T. *J. Am. Chem. Soc.* **1985**, *107*, 4192-4199. (b) Askew, B.; Ballester, P.; Buhr, C.; Jeong, K. S.; Jones, S.; Parris, K.; Williams, K.; Rebek, J., Jr. *J. Am. Chem. Soc.* **1989**, *111*, 1082-1090. (c) Maverick, A. W.; Buckingham, S. C.; Yao, Q.; Bradbury, J. R.; Stanley, G. G. *J. Am Chem. Soc.* **1986**, *108*, 7430-7431 and references therein. Studies of isomerization in dimers have also been restricted to relatively rigid systems: (d) Brown, A. B.; Whitlock, H. W. *J. Am. Chem. Soc.* **1989**, *111*, 3640-3651, and references therein.

(2) Other examples of porphyrin host-guest chemistry include the following: (a) Collman, J. P.; Hendricks, N. H.; Leidner, C. R.; Ngameni, E. *Inorg. Chem.* **1988**, *27*, 387-393. (b) Hamilton, A. D.; Lehn, J.-M.; Sessler, J. L. *J. Am. Chem. Soc.* **1986**, *108*, 5158-5167. (c) Tabushi, I.; Kugimiya, S.; Kinnaird, M. G.; Sasaki, T. *J. Am. Chem. Soc.* **1985**, *107*, 4192-4199. (d) Danks, I. P.; Sutherland, I. O.; Yap, C. H. *J. Chem. Soc., Perkin Trans. 1* **1990**, *421*-422.

(3) Anderson, H. L.; Hunter, C. A.; Meah, M. N.; Sanders, J. K. M., following paper in this issue.

(4) Hunter, C. A.; Sanders, J. K. M. *J. Am. Chem. Soc.* **1990**, *112*, 5525-5534.

(5) Leighton, P.; Cowan, J. A.; Abraham, R. J.; Sanders, J. K. M. *J. Org. Chem.* **1988**, *53*, 733-740.

(6) Hunter, C. A.; Leighton, P.; Sanders, J. K. M. *J. Chem. Soc., Perkin Trans. 1* **1989**, 547-552.

(7) Hunter, C. A.; Sanders, J. K. M.; Stone, A. J. *J. Chem. Phys.* **1989**, *133*, 395-404.

0002-7863/90/1512-5773$02.50/0 

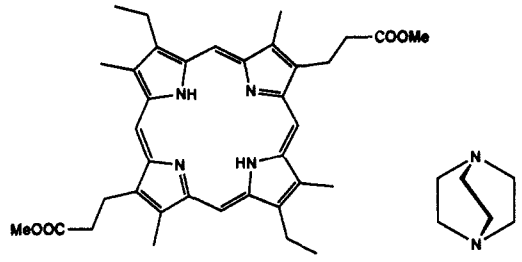


3 4

Accurately determined DABCO solutions of between $10^{-5}$ and $10^{-3}$ M were made up in 1-mL volumetric flasks and titrated into the porphyrin sample in 1-μl aliquots via a 10-μL Hamilton 800 Series syringe. The analysis of the results allowed for the changes in volume which occurred during the titration. For variable-temperature UV–vis experiments, accurately measured mixed ligand-porphyrin solutions were made up such that the ratio of free/bound porphyrin was ca. 1. The absorbance of this mixture was recorded at two wavelengths (usually the absorption maxima of the free and bound species) and at 20 different temperatures in the range 0–35°C. Titration data were analyzed by graphical and curve-fitting programs on a Macintosh SE microcomputer. The curve-fitting programs are based on Simplex routines written by Dr. A. Crawford.

$^1$H NMR spectra were recorded on Bruker AM-400 and WH-250 spectrometers. Spectra were obtained in deuteriodichloromethane or $C_2D_2Cl_4$ solutions. One-dimensional spectra were typically acquired by using 16K data points with a spectral width of 18 ppm. Two-dimensional COSY and NOESY spectra were acquired in the phase-sensitive mode by using standard software packages. Typically 2K data points were used in f2, and 512 or 1024 increments were acquired in f1 with a spectral width of 18 ppm in each dimension. Either 16 or 32 free induction decays were acquired in each increment. Zero-filling was used in f1 but not in f2, and suitable apodization was applied in processing spectra.

## Results and Discussion

In order to understand the behavior of the dimer–DABCO complexes, we first describe how DABCO binds to monomeric metalloporphyrins, by using UV–visible absorption and $^1$H NMR spectroscopy as probes: the former was used to elucidate the stoichiometry of binding, the binding energy, and a limited amount of structural data, while the latter yielded more detailed information about the geometry of the complexes and the kinetics of the ligand-exchange processes. UV–visible absorption spectroscopic measurements were made at porphyrin concentrations of ca. $10^{-6}$ M, and NMR measurements were made at ca. $10^{-3}$ M leading to major differences in the complexes observed.

**Ternary Porphyrin–DABCO Complexes.** Titration of DABCO with **Zn3** was followed by UV–visible absorption spectroscopy, by using the coordination shift of the Soret absorption (Table I).[1a,5] Analysis of the binding curve showed that a simple 1:1 complex was formed with a binding constant of $2.4 \times 10^5$ M$^{-1}$ (Table II). This was expected as zinc in porphyrins is almost exclusively five-coordinate. A variable-temperature experiment gave $\Delta H$ = −62 kJ mol$^{-1}$ (15 kcal mol$^{-1}$) and $\Delta S$ = −103 J K$^{-1}$ mol$^{-1}$ (±5%) for the binding process.

When this titration was repeated at $10^{-3}$ M and followed by using $^1$H NMR spectroscopy, different behavior was observed. In the presence of less than 1 equiv of the ligand, a *ternary complex* or *sandwich dimer* was formed (Figure 2), and the equilibria illustrated in Figure 3 were observed. When more than 1 equiv of ligand had been added, only the simple 1:1 binary complex was observed as in the UV–v experiment. The $^1$H NMR resonances of the sandwich dimer were broad at room temperature but were characterized by a DABCO methylene signal at ca. −5 ppm; the shift from free ligand, $\Delta\delta$, is −8.0 ppm. The sandwich dimer also showed resonances at ca. 9.5 ppm due to the porphyrin meso protons ($\Delta\delta$ = −0.50 ppm) and at ca. 3.4 ppm due to the porphyrin ring methyls ($\Delta\delta$ = −0.3 ppm). The proximity of the two porphyrin π-systems in this complex causes these signals to experience large upfield ring current induced shifts relative to the corresponding signals in the binary **Zn3**–quinuclidine (**5**) and **Zn3**–DABCO complexes (Table III). The chemical shifts agree well with values predicted by ring current calculations.[5] For a

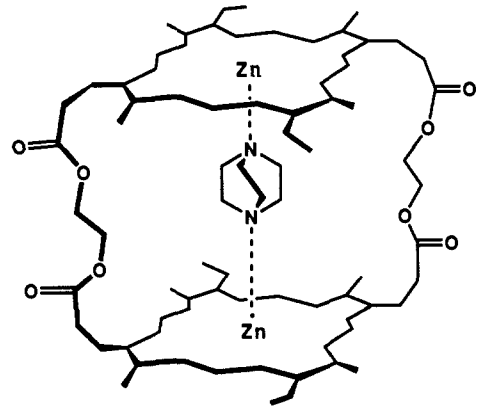


**Figure 1.** The $Zn_2$**1**–DABCO complex. For clarity, bonds and atoms within the porphyrin moiety have not been included in the figures.

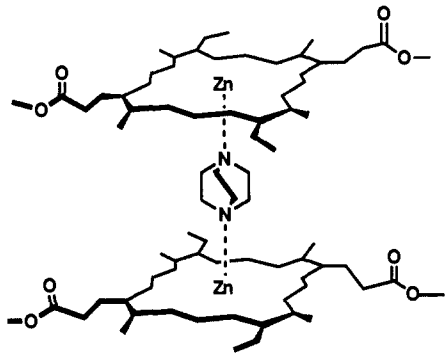


**Figure 2.** A sandwich dimer: the ternary $(Zn3)_2$–DABCO complex.

**Table I.** UV-Visible Absorption Spectra: Data for the Soret Band Absorption

| porphyrin[a] | $\lambda_{max}$ (nm) | $\epsilon \times 10^{-3}$ | FWHM[b] (nm) |
|---|---|---|---|
| $Zn_2$**1** | 388 | 272 | 28 |
| $Zn_2$**2** | 388 | 166 | 31 |
| **Zn3** | 402 | 314 | 13 |
| $Zn_2$**1** + **4** | 409 | 434 | 12 |
| $Zn_2$**2** + **4** | 409 | 324 | 13 |
| **Zn3** + **4** | 415 | 320 | 12 |

[a] All measurements were made on $CH_2Cl_2$ solutions ca. $10^{-6}$ M in porphyrin. [b] Full width at half maximum of the Soret absorption.

**Table II.** Binding Constants (in M$^{-1}$)

| | ligand | | |
|---|---|---|---|
| | pyridine | | DABCO |
| porphyrin[a] | $K_1$ | $K_2$ | $K$ |
| $Zn_2$**1** | $1.05 \times 10^2$ | $2.02 \times 10^2$ | $7.39 \times 10^7$ |
| $Zn_2$**2** (isomer 1) | | | $\approx 1 \times 10^6$ |
| | $1.02 \times 10^2$ | $2.2 \times 10^1$ | |
| $Zn_2$**2** (isomer 2) | | | $\approx 1 \times 10^7$ |
| **Zn3** | $2.89 \times 10^3$ | | $2.4 \times 10^5$ |

[a] All measurements were made on $CH_2Cl_2$ solutions ca. $10^{-6}$ M in porphyrin.

parallel arrangement of the porphyrins with an interplanar separation of 7 Å, our calculations predict the following upfield shifts relative to free ligand: $\Delta\delta$(DABCO) = −7.9, $\Delta\delta(H_{meso})$ = −0.57, and $\Delta\delta$(P–Me) = −0.32 ppm.

The bound DABCO methylene chemical shifts can be compared with the chemical shifts of the methylene groups of quinuclidine when it is bound to **Zn3** (Figure 4). The change in DABCO chemical shift when it is bound between the two porphyrins is simply the sum of the shifts induced by the two ring currents:

$$\Delta\delta(\text{DABCO}) = -8.0 \text{ ppm} \approx \Delta\delta(\textbf{5}\text{-}H_\alpha) + \Delta\delta(\textbf{5}\text{-}H_\beta) = -5.8 + (-2.1) \text{ ppm} = -7.9 \text{ ppm}$$

We have used this chemical shift information as a diagnostic tool

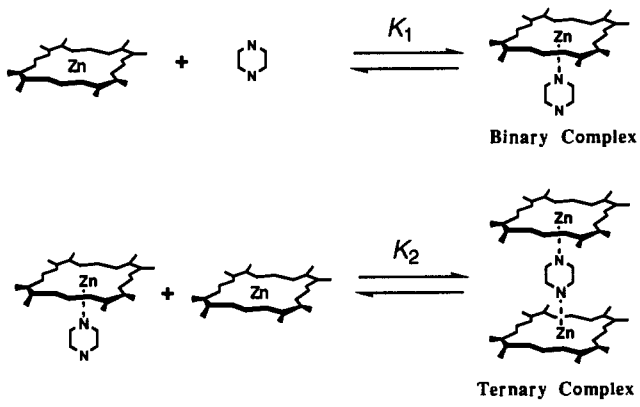


**Figure 3.** Binding equilibria for a monomeric zinc porphyrin and DABCO.

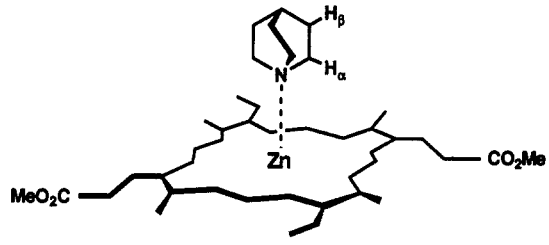


**Figure 4.** The **Zn3–5** complex.

**Table III.** Selected $^1$H NMR Chemical Shifts of Porphyrin Complexes (in ppm)

| | complex[a] | | | | |
|---|---|---|---|---|---|
| | | | $Zn_2$**2** + **4** | | |
| signal[b] | **Zn3** + **5** | $Zn_2$**1** + **4** | isomer 1 | isomer 2 | $(Zn3)_2$ − **4** |
| $H_{meso}$ | | | | | 9.5 |
| $H_5$ | 9.98 | 9.52 | 9.71 | 9.52 | |
| $H_{10}$ | 9.94 | 9.48 | 9.48 | 9.43 | |
| P-Me | 3.69 | 3.37 | 3.39 | 3.37 | |
| | 3.64 | 3.37 | 3.37 | 3.33 | |
| 4-$CH_2$ | | −5.20 | −5.52 | −5.53 | −5.0 |
| | | −5.25 | | | |
| | | −5.30 | | | |
| 5-$H_\alpha$ | −3.49 | | | | |
| 5-$H_\beta$ | −0.64 | | | | |

[a] All measurements made on $CH_2Cl_2$ solutions ca. $10^{-3}$ M in porphyrin. [b] The structures and Figure 4 illustrate the proton-labeling scheme used.

in identifying such DABCO–metalloporphyrin sandwich dimer complexes.

Many other zinc porphyrins form similar sandwich dimer complexes with DABCO. At concentrations of ca. $10^{-3}$ M, ZnOEP (**Zn6**) in the presence of 0.5 equiv of DABCO forms a sandwich dimer (Figure 2). The chemical shifts of the porphyrin meso and the DABCO methylene signals are again highly diagnostic of this structure. At room temperature, the signals were exchange broadened, but at −70 °C a slow exchange limit was reached in which the porphyrin $CH_2$ protons became nonequivalent, and this signal split into a complex multiplet. Similar splitting has been observed many times in porphyrin systems with two inequivalent faces.[8]

An equimolar solution of two different zinc porphyrins and DABCO generally contains a statistical mixture of three sandwich dimers: the DABCO signals in the low-temperature $^1$H NMR spectrum reveal 1 equiv each of the two simple sandwich dimers and 2 equiv of the mixed sandwich dimer. When a 1:1:1 mixture of **Zn6**, **Zn7**,[9] and DABCO was examined at −70 °C, four bound DABCO signals were observed, with relative intensities 1:1:1:1. A signal at −5.72 ppm was due to the **Zn6** sandwich dimer, that

(8) See, for example: Ganesh, K. N.; Sanders, J. K. M.; Waterton, J. C. *J. Chem. Soc., Perkin Trans. 1* **1982**, 1617–1624.
(9) Billig, M. J.; Baker, E. W. *Chem. Ind. (London)* **1969**, 654–655.

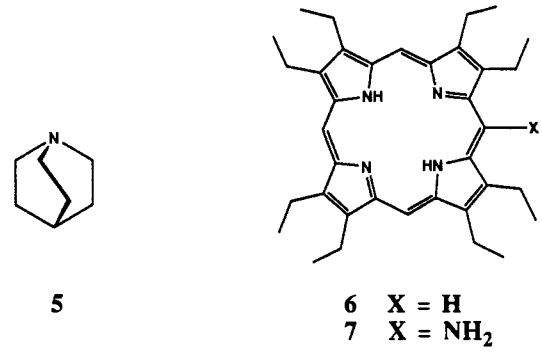


**5** **6** X = H **7** X = $NH_2$

at −4.60 ppm was due to the **Zn7** sandwich dimer, and the remaining two signals at −4.78 and −5.54 ppm were due to the mixed sandwich dimer. The amino group reduces the porphyrin ring current, and so, in the mixed dimer, the two ends of the bound DABCO are nonequivalent. On cooling this solution further, coupling was resolved in the mixed-dimer ligand signals: the DABCO methylene signals were triplets as expected.

These systems provide some exciting possibilities for the construction of porphyrin supramolecules. The formation of such complexes indicates that the second nitrogen of DABCO remains basic when the other nitrogen is coordinated to a metal: the fact that we can detect only the ternary complex when 0.5 equiv of ligand is added to a $10^{-3}$ M zinc porphyrin solution indicates that, for binding at the second nitrogen of DABCO, $K_2 \geq 10^4$ $M^{-1}$ (Figure 3). In separate experiments we have measured $K_2$ and hence quantified the cooperativity $\alpha(=4K_2/K_1)$ between the two ends of the bifunctional ligand.[3]

**Complexes of $Zn_2$1 and DABCO.** The $^1$H NMR and UV-visible absorption spectra of $Zn_2$**1** have already been described in detail.[5] $Zn_2$**1** is a 1:1 mixture of "meso" and "racemic" isomers. At room temperature, these isomers are in fast exchange on the $^1$H NMR chemical shift time scale, but at −70 °C the slow exchange spectrum is obtained. This interpretation differs from that in our previous paper.[10] The two isomers have almost identical properties with respect to DABCO binding.

**UV-Visible Absorption Spectroscopy.** On addition of DABCO, the Soret peak moved from 388 to 409 nm and sharpened (Table I). Good isosbestic points were observed, and a Hill plot[11] of ln $\{(A_0 - A)/(A - A_f)\}$ versus ln [DABCO] yielded a straight line of slope 1.[12] This indicates a simple binding process with the formation of a 1:1 complex. The binding constant is $7.39 \times 10^7$ $M^{-1}$, which is significantly higher than the binding constant for the **Zn3**–DABCO complex (Table II). The 1:1 dimer complex persisted even in the presence of 1000-fold excess of ligand; we have never detected binding of a second DABCO. A variable-temperature experiment gave the thermodynamic parameters for binding, $\Delta H = -77 \pm 8$ kJ mol$^{-1}$ and $\Delta S = -121 \pm 12$ J K$^{-1}$ mol$^{-1}$. The low precision of these values results from the exceptionally high binding constant; very dilute solutions had to be used, giving small spectral changes. The significance of these measurements will be discussed in detail below.

Exciton coupling of the two chromophores in this complex causes a blue-shift of the Soret band to 409 nm from the usual value of 415 nm for a zinc porphyrin–DABCO complex (Table I). Our theoretical study[7] has shown that this shift is consistent with the geometry shown in Figure 1: the two porphyrin $\pi$-systems are held parallel at an interplanar separation of 7 Å and with no offset in the plane of the porphyrins. This is also the geometry predicted by models.

(10) The minor signals we originally attributed to the racemic isomer actually belong to a cyclic tetramer which can be separated by careful chromatography. The geometrical conclusions of our previous paper are unchanged, but we now interpret the low-temperature spectrum of $Zn_2$**1** as demonstrating slow exchange between "racemic" and "meso" isomers in addition to a temperature-dependent geometry.
(11) Hill, A. V. *J. Physiol. London* **1910**, *40*, IV–VII.
(12) $A_0$ is the absorption of the free dimer at wavelength, $\lambda$. $A_f$ is the absorption of the bound complex at $\lambda$. $A$ is the absorption measured at $\lambda$ for a concentration of ligand given by [DABCO].

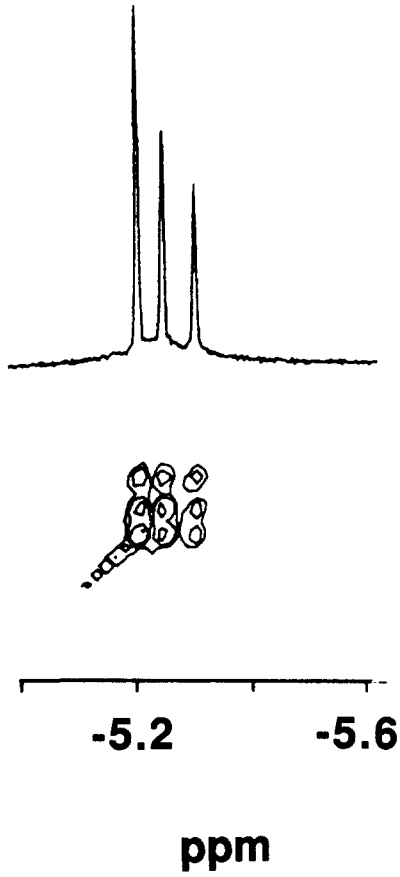


**Figure 5.** The bound DABCO methylene region of a room temperature NOESY spectrum of $Zn_2$**1** in the presence of 0.5 equiv of DABCO in $CD_2Cl_2$.

**$^1$H NMR Spectroscopy: Nature of the Complexes.** In the presence of between 1 and 50 equiv of DABCO, the $^1$H NMR spectrum of $Zn_2$**1** shows that DABCO is bound inside the cavity of the porphyrin dimer (Figure 1). The characteristic changes in the chemical shifts of the porphyrin meso, ring methyl, and the DABCO signals (Table III) show that the geometry of the complex is effectively identical with the ternary sandwich dimer complexes discussed above. The bridging chains are long enough to allow the dimer to achieve the optimum geometry for accommodating DABCO in the cavity.

When a titration of DABCO with $Zn_2$**1** was followed with $^1$H NMR spectroscopy, the porphyrin and ligand free and bound signals were all in slow exchange as a result of the very large binding constant. In the presence of up to 0.5 equiv of DABCO there were three bound DABCO signals at −5.20, −5.25, and −5.30 ppm (Table III). A COSY spectrum showed no coupling between these signals, while a NOESY spectrum indicated that they were all exchanging with each other (Figure 5). The latter spectrum was acquired in the phase-sensitive mode, so that chemical exchange cross-peaks, such as these, appeared negative, while genuine NOE cross-peaks appeared positive. This observation suggested that there were three different species present in which DABCO was bound between two porphyrin moieties. A variable-temperature experiment showed that the −5.30 ppm DABCO signal exchanged faster than the other two bound DABCO signals and so probably belonged to a different type of complex. The activation energy for the "off" process (the exchange between free and bound DABCO) for this signal was ca. 55 kJ mol$^{-1}$ compared with 70 kJ mol$^{-1}$ for the other two signals (Table IV). Comparison of the behavior of the −5.30 ppm signal with the behavior of the ternary sandwich dimer complexes suggested that this signal arose from the ternary $Zn_2$**1**–DABCO–$Zn_2$**1** complex, illustrated in Figure 6; dissociation of this ternary complex is entropically more favorable than dissociation of the binary complex, so the activation energy is lower (see below). The larger upfield ring current

**Table IV.** Activation Energies for the Chemical Exchange Processes in the $Zn_2$**1**–DABCO Binary Complex

| signal[a] | exchange process | $\Delta\delta^b$ (ppm) | $T_c^c$ (K) | $\Delta G^*$ (kJ mol$^{-1}$) |
|---|---|---|---|---|
| bound $H_5$ | meso ↔ racemic | 0.01 | 308 | 70 |
| bound $H_{10}$ | meso ↔ racemic | 0.01 | 308 | 70 |
| bound 4 $CH_2$ | meso ↔ racemic | 0.05 | 328 | 68 |
| $H_5$ | free ↔ bound | 0.35 | 340 | 68 |
| 4 $CH_2$ | free ↔ bound | 8.01 | 366 | 65 |

[a] All measurements made on a $C_2D_2Cl_4$ solution ca. $2 \times 10^{-3}$ M in $Zn_2$**1** with 0.5 equiv of ligand present. [b] Difference in chemical shift of the two exchanging signals. [c] Coalescence temperature.

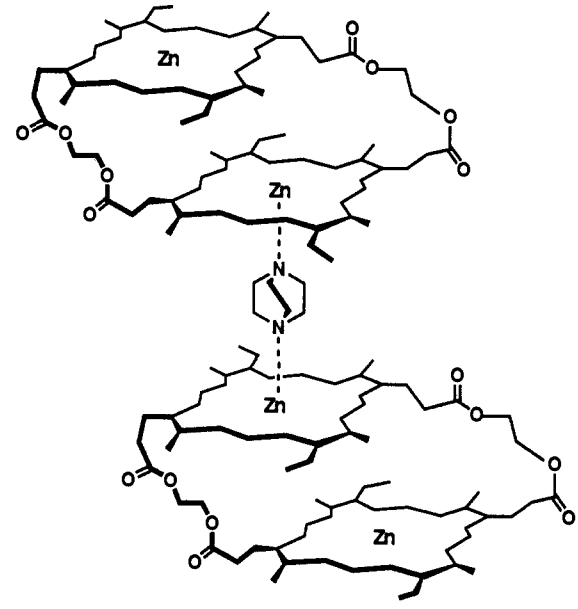


**Figure 6.** The ternary $(Zn_2\mathbf{1})_2$–DABCO complex.

induced shift experienced by this signal is consistent with the additional ring current effects of the two extra but distant porphyrins in this complex. This interpretation was confirmed by adding increasing amounts of DABCO. As the ratio of DABCO/$Zn_2$**1** was increased above 0.5, the upfield DABCO signal gradually disappeared, until, in the presence of 1 equiv of ligand, only two bound DABCO signals were observed. The disappearance of this signal parallels the observations made on the ternary sandwich dimers.

The formation of the tetraporphyrin complex can be explained by using the binding constants measured by UV–visible spectroscopy. Allowing for the cooperativity in the second binding constant of DABCO, $\alpha$, the ratio of the ternary $Zn_2$**1**–DABCO–$Zn_2$**1** complex (Figure 6) to the binary $Zn_2$**1**–DABCO complex (Figure 1) in the presence of excess porphyrin is given by

$$\frac{[Zn_2P\text{–DABCO–}Zn_2P\text{ complex}]}{[Zn_2P\text{–DABCO complex}]} = \frac{\alpha K_{out}^2[Zn_2P]}{4K_{in}} \quad (1)$$

where $Zn_2P$ represents a bis zinc porphyrin dimer; $\alpha = 0.80^3$; $K_{in} = 7.39 \times 10^7$ M$^{-1}$, the binding constant for binding *inside* the dimer; and $K_{out}$ is the binding constant for the 1:1 complex with DABCO bound on the *outside* of the dimer (cf. $K_1$ in Figure 3), i.e., $K_{out} \approx 2.4 \times 10^5$ M$^{-1}$, the binding constant for binding of DABCO to the monomer, **Zn3**. For solutions approximately $10^{-3}$ M in porphyrin, the above expression gives the ratio of ternary/binary complex to be of the order of one, as observed.

The remaining two bound ligand signals correspond to complexes in which the DABCO is bound inside the cavity of $Zn_2$**1**. This dimer exists as two diastereomers which are present in equal amounts and which interconvert by rotation of one porphyrin relative to the other; these two isomers give rise to the two observed forms of the DABCO complex. The isomers behave identically when observed by UV–visible absorption spectroscopy; the Soret bandwidth of the $Zn_2$**1**–DABCO complex is the same as that of

the **Zn3**–DABCO complex (Table I), indicating that the two isomeric complexes have a similar porphyrin–porphyrin geometry, and a Hill plot of the titration data shows that, within experimental error, they have identical binding constants. Although the geometry of these complexes is similar, NMR shows that the two isomers adopt slightly different geometries when they bind DABCO; there is a 1% change in the change in chemical shift, $\Delta\delta$, due to the difference betweeen the two geometries. This difference could be the result of a rotation of the porphyrin rings relative to each other or due to a small change in the interplanar separation of the $\pi$-systems.

This isomer hypothesis is verified by the meso region of the $^1$H NMR spectrum (not shown). At room temperature in $CD_2Cl_2$ and in the presence of 0.5 equiv of ligand, two free and two bound meso signals were observed in slow exchange. By using chemical exchange cross-peaks in the NOESY spectrum, we were able to assign these signals (Table III); in this room temperature spectrum, the bound signals were two singlets corresponding to the two meso protons, $H_5$ and $H_{10}$. On cooling to −15 °C, each of these signals split into two singlets separated by 0.01 ppm. The two sets of signals arising from this splitting correspond to the two forms of the complex observed in the DABCO region of the spectrum. Cooling to −70 °C produced no further changes in the spectrum.

The ternary complex was not observed in the meso region of the spectrum. In monomer ternary complexes, the meso protons were upfield shifted by 0.3 ppm; in the ternary complex of $\mathbf{Zn_21}$, the corresponding protons will be in exchange both with free $\mathbf{Zn_21}$ and with the uncomplexed moiety of the ternary complex (Figure 6). Thus the "free" meso signals are actually the fast exchange average of free and ternary complex, but, as the latter was never more than 10% of the total porphyrin concentration, the shift and broadening are negligible.

Strikingly, when $C_2D_2Cl_4$ was used as the solvent, the four bound meso signals (due to slow exchange between the two isomeric complexes) were observed at room temperature. Possibly the 4-fold greater viscosity of $C_2D_2Cl_4$ than $CD_2Cl_2$ slows down the rate of chemical exchange; this suggests that the exchange process involves the displacement of a large volume of solvent, such as would be caused by the rotation of one of the porphyrin moieties relative to the other, i.e., exchange between "meso" and "racemic" isomers.

The rest of the $^1$H NMR spectrum is complicated and has not been assigned or interpreted fully. However, the chemical exchange cross-peaks in the NOESY spectrum give some chemical shift information about the bound complexes. The bridging $OCH_2CH_2O$ group in the bound species show multiplets shifted upfield relative to the free signal (singlet at 4.51 ppm) by 0.4, 0.7, and 0.9 ppm. The upfield shift of the bridging group signals is consistent with cavity opening, since this process pulls these groups into the region between the two porphyrins where they experience larger ring currents. The implication is that the complexes have highly defined structures, with the bridging chains extended so that they have little flexibility.

**$^1$H NMR Spectroscopy: Exchange Processes.** A variable-temperature study was carried out for a $C_2D_2Cl_4$ solution of $\mathbf{Zn_21}$ containing 0.5 equiv of ligand. The temperatures for the coalescences of four sets of exchanging signals were determined, and the corresponding activation energies were calculated by using simple transition-state theory for unimolecular reactions (Table IV).[13] Two exchange processes cause the observed coalescence: exchange between the two diastereomeric forms of the DABCO complex and exchange between free and bound species. Exchange between the free and bound species was observed as coalescence of the free and bound DABCO signals and coalescence of the free and bound $H_5$ meso signals. Exchange between the meso and racemic isomers of the complex was observed as coalescence of the two bound DABCO signals at −5.20 and −5.25 ppm and coalescence of the two sets of bound meso signals (the two signals at 9.52 ppm coalesce as do the two at 9.48 ppm).[14] The activation

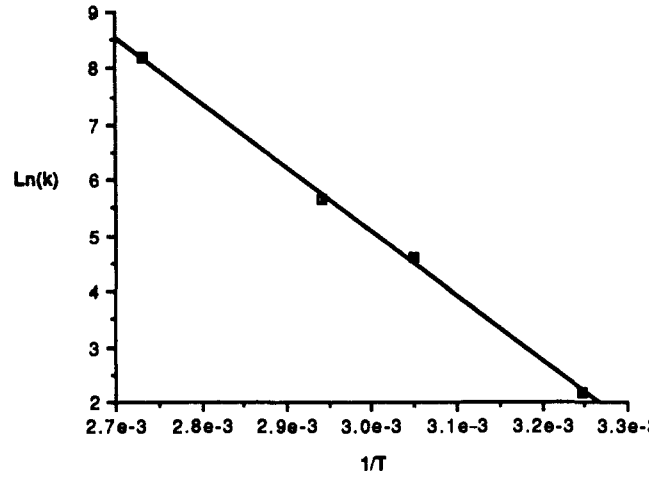


**Figure 7.** Arrhenius plot for the chemical exchange processes in a 2:1 mixture of $\mathbf{Zn_21}$ and DABCO.

energies for these four processes are close in value, indicating that they are all due to the same exchange process. In other words, exchange between the free and bound and the meso and racemic forms is the same process. This is supported by the good fit of the data to an Arrhenius plot (Figure 7) which gives the following parameters for the unimolecular exchange process at 300 K:

$$\Delta G^{\ddagger} = 70.4 \text{ kJ mol}^{-1} \qquad \Delta H^{\ddagger} = 94 \text{ kJ mol}^{-1}$$
$$\Delta S^{\ddagger} = 77 \text{ J K}^{-1} \text{ mol}^{-1}$$

The activation energy calculated is for dissociation of the $\mathbf{Zn_21}$–DABCO complex since this is the slowest process (Figure 8). The value of $\Delta S^{\ddagger}$ indicates that, as expected, the transition state is disordered relative to the bound complex and ordered relative to the free species ($\Delta S$(binding) $\approx -120$ J K mol$^{-1}$). $\Delta H^{\ddagger}$ shows that there is a large enthalpic barrier to the "off" process: the rate-limiting step involves cleavage of at least one zinc–nitrogen bond and binding studies on **Zn3** showed that $\Delta H$ for breaking a zinc–DABCO bond is 62 kJ mol$^{-1}$. There may also be some unfavorable strain of the bridging side chains in the transition state, but models suggest that this will be a minor contribution.

It is not possible to calculate accurately the activation energy for the chemical exchange process between the uncomplexed meso and racemic isomers because the geometry of the dimers appears to vary with temperature and hence the chemical shifts of the two slow exchange forms change on cooling.[5] However, from the chemical shift differences between the slow exchange signals in the meso region of the spectrum and the coalescence temperature for exchange of these signals,[5] we estimate the activation energy as approximately 49 kJ mol$^{-1}$. The fact that this activation energy for chemical exchange between the two uncomplexed isomers of $\mathbf{Zn_21}$ is ca. 21 kJ mol$^{-1}$ less than that for exchange between the two bound isomers indicates that it is indeed ligand-metal bond breaking that is the rate-limiting process shown in Figure 8. Rotation of one porphyrin relative to another does not present an energetic barrier to the dissociation of the $\mathbf{Zn_21}$–DABCO complex.

We have not been able to measure the activation energy for the "on" process for DABCO binding to $\mathbf{Zn_21}$. However binding to $10^{-7}$ M dimer when observed by UV–visible absorption spectroscopy is complete in less than a minute, setting 41 kJ mol$^{-1}$ (10 kcal mol$^{-1}$) as an upper limit for the barrier to binding inside the cavity. This is lower than both the activation energy for $\mathbf{Zn_22}$–DABCO binding (discussed below) and for exchange be-

(13) Sandström, J. *Dynamic NMR Spectroscopy*; Academic Press: London, 1982, pp 77–123.

(14) The coalescence of the two sets of bound meso signals, each separated by 0.01 ppm, might be thought questionable since any small increase in line width would look like exchange coalescence. However, we also observe coalescence of these signals in $CD_2Cl_2$ solution, indicating that this is genuinely due to exchange between the two isomers. Also this point falls on the same straight line as the other three in the Arrhenius plot (Figure 7).

(15) White, W. I. *The Porphyrins, Vol. V*; Dolphin, D., Ed.; Academic Press: New York, 1978, pp 303–339.

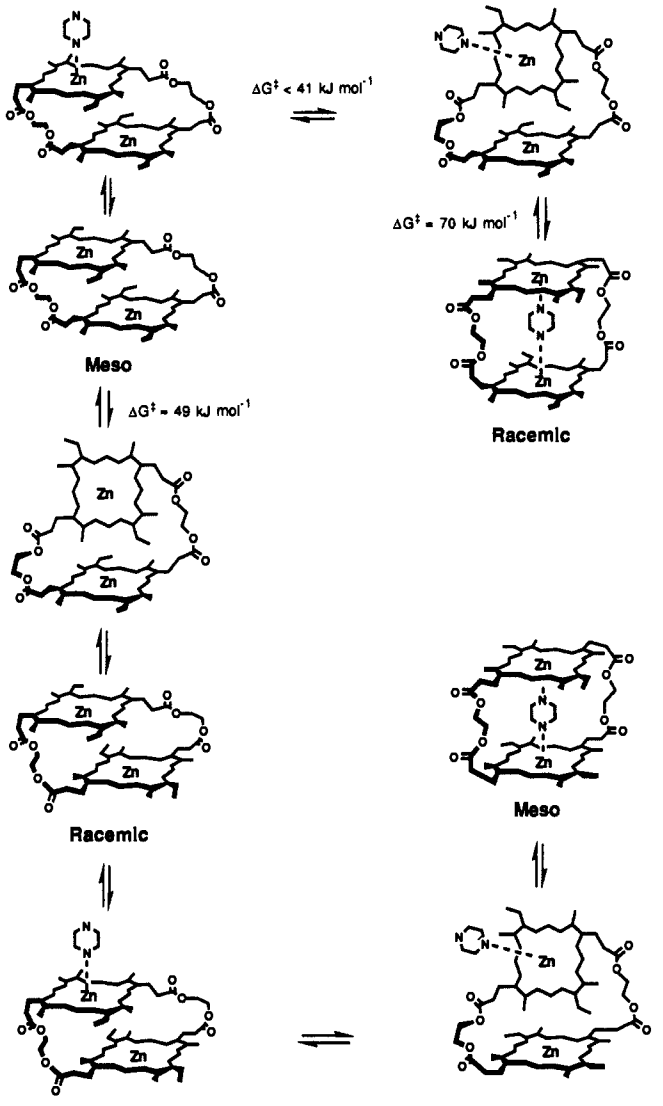


**Figure 8.** The exchange processes for the binary $Zn_2$**1**–DABCO complex in the presence of excess porphyrin.

tween the two isomers of uncoordinated $Zn_2$**1**. The energetic barrier to the "on" processes and to exchange between the meso and racemic isomers can be ascribed to the attractive $\pi$–$\pi$ interactions between the two porphyrins (see below), and so binding DABCO on the outside of $Zn_2$**1** must have reduced the $\pi$–$\pi$ interaction in this system. This is the same effect as disaggregation of metalloporphyrins by ligand coordination.[6] Thus the rate-determining step for insertion of the DABCO into the cavity is opening of the cavity after DABCO is bound on the outside (Figure 8). Coordination of DABCO on the outside of the dimer catalyzes rotation of one porphyrin and binding of DABCO inside the cavity. A corollary is that binding on the outside of the uncomplexed meso isomers leads to formation of the racemic complex and vice versa. The mechanism which accounts for these observations is summarized in Figure 8.

At room temperature, and while there was less than 1 equiv of DABCO present, the two bound downfield DABCO signals were sharp (in slow exchange), and the line widths were independent of the concentration of ligand. This indicates that the exchange rate was effectively constant throughout this early part of the titration, confirming that the chemical exchange process was the simple unimolecular process discussed above. However, as more DABCO was added, once the ratio DABCO/$Zn_2$**1** exceeded one, the bound DABCO signals broadened. The line width increased markedly as the concentration of DABCO was increased further (Figure 9), the exchange rate being approximately proportional to the concentration of free ligand. The exchange process was now bimolecular: a second molecule of DABCO binding to

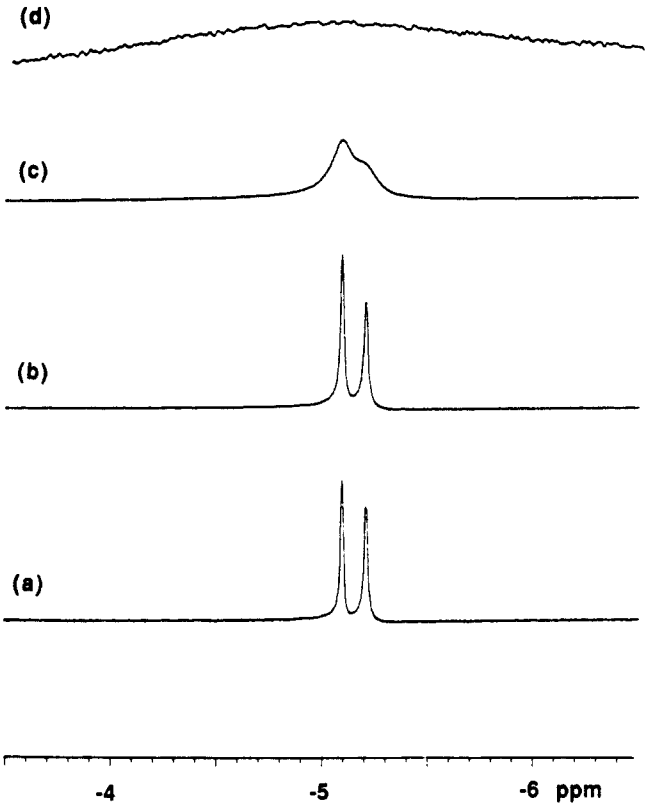


**Figure 9.** Dependence of the DABCO methylene region of the room-temperature $^1$H NMR spectrum of the $Zn_2$**1**–DABCO complex in $C_2D_2Cl_4$ on the ratio [$Zn_2$**1**]/[DABCO]: (a) 1.1, (b) ≈ 0.7, (c) 0.4, and (d) 0.2.

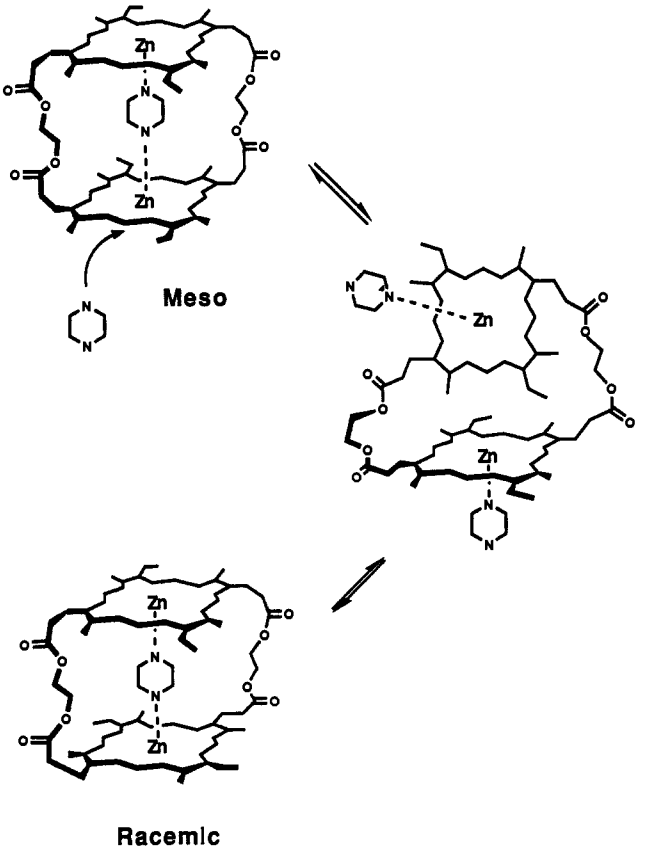


**Figure 10.** The exchange processes for the binary $Zn_2$**1**–DABCO complex in the presence of excess DABCO.

the outside of the complex and assisting the first zinc–nitrogen bond cleavage in the dissociation of the complex (Figure 10).

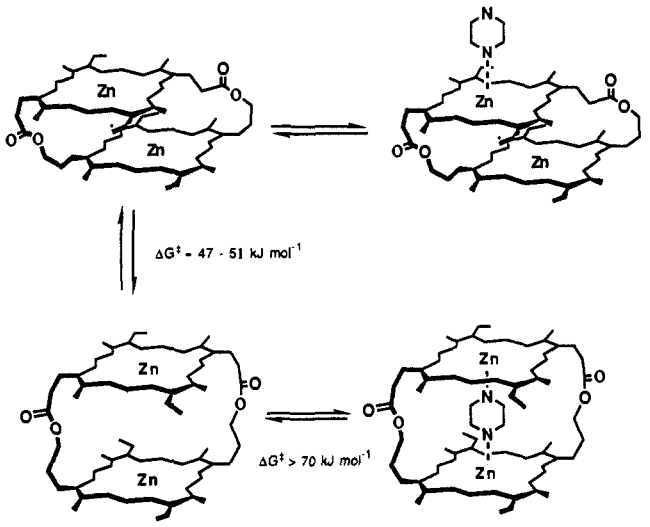


**Figure 11.** The exchange processes for the binary $Zn_22$–DABCO complex.

**Complexes between $Zn_22$ and DABCO.** We also studied the more complicated binding of DABCO inside the cavity of the smaller dimer, $Zn_22$. Again there are two isomers, the "syn" and "anti" forms, but the bridging straps are now too short to allow interconversion. The thermodynamics and kinetics of DABCO binding are remarkably different in these two isomeric systems. We have not separated the two isomers, all measurements being made on a 3:2 mixture.

**UV–Visible Absorption Spectroscopy.** In the presence of a large excess of DABCO the UV–visible absorption spectrum of $Zn_22$ was identical with that of the $Zn_21$–DABCO complex (Table I), and again a second ligand did not bind even in 1000-fold excess of DABCO. However, the binding was remarkably slow: at $10^{-7}$ M DABCO, the equilibration time for binding was greater than a week; in all other ligand–zinc porphyrin systems we have studied, binding has been essentially instantaneous. From the titration curve, we have estimated the binding constants for the two isomers to be ca. $1 \times 10^6$ and $1 \times 10^7$ $M^{-1}$ (Table II). One isomer accommodates DABCO more readily than the other, but for both the binding is weaker than for $Zn_21$, suggesting that there is strain associated with DABCO binding inside $Zn_22$.

The binding kinetics for the two isomers are also different. A plot of ln(rate/[free dimer]) versus ln([DABCO]) indicates that the binding process for each isomer is essentially bimolecular, with rates for the "on" processes of ca. $5 \times 10^4$ $s^{-1}$ $M^{-1}$ for one isomer and ca. $1 \times 10^5$ $s^{-1}$ $M^{-1}$ for the other, corresponding to energetic barriers of ca. 47 and 51 kJ $mol^{-1}$. These low rate constants are a consequence of the mechanism illustrated in Figure 11: because the two porphyrins in $Zn_22$ cannot rotate relative to one another, *binding of DABCO on the outside of the dimer can never lead to binding inside the cavity*. The cavity must first open to make enough space for the DABCO to penetrate.

**$^1$H NMR Spectroscopy.** The $^1$H NMR spectrum of $Zn_22$ in the presence of excess DABCO was similar to that of the $Zn_21$–DABCO complex. It was assigned by using a NOESY spectrum. The chemical shifts of the porphyrin meso, ring methyl, and the DABCO bound signals are all diagnostic of a 1:1 complex with DABCO bound inside the cavity of the dimer (Table III). However, while one of the isomers of $Zn_22$ (denoted "isomer 2") attains the optimum geometry for accommodating DABCO inside the cavity, the other (denoted "isomer 1") cannot. The chemical shifts of the porphyrin meso signals demonstrate that the "isomer 1" complex has a slightly different geometry for the other porphyrin–DABCO–porphyrin systems (Table III). This probably accounts for the difference in the binding properties of the two isomers.

In contrast to $Zn_21$, the $^1$H NMR spectrum was very broad in the presence of up to 0.5 equiv of ligand: two broad bound meso signals at ca. 9.5 ppm and a bound DABCO signal at ca. −5 ppm are observed. This spectrum is characteristic of a ternary complex,

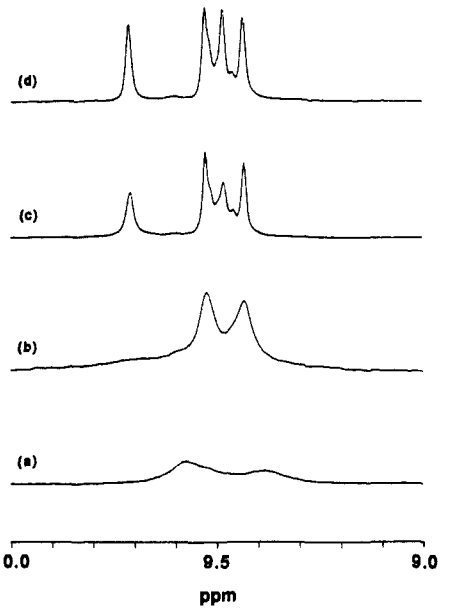


**Figure 12.** Dependence of the DABCO methylene region of the room-temperature $^1$H NMR spectrum of the $Zn_22$–DABCO complex in $CD_2Cl_2$ as a function of the ratio [$Zn_22$]/[DABCO]: (a) 5, (b) 2.0, (c) 1.6, and (d) 1.0.

and the porphyrin signals are consequently in fast exchange and broadened. For the two isomers of $Zn_22$, $K_{in} \approx 1 \times 10^6$ and $1 \times 10^7$ $M^{-1}$, and so, for a $10^{-3}$ M porphyrin solution, eq 1 predicts the ratio of ternary/binary complex to be between 7 and 70. So, until the ratio of [DABCO]/[$Zn_22$] exceeded 0.5, the ternary complex dominated the spectrum. As the ratio of [DABCO]/[$Zn_22$] increased from 0.5 to 1, the two broad meso signals of the ternary complex were replaced by the sharp well-resolved slow exchange signals of the binary complexes (Figure 12). However, initially only the meso signals of "isomer 2" appeared, and only when all of this isomer had formed the binary complex with DABCO did we observe the signals due to the "isomer 1"–DABCO binary complex. DABCO preferentially binds to "isomer 2", and only when all of this isomer is bound does it bind to "isomer 1". The isomer of $Zn_22$ which has the highest binding constant ("isomer 2") is the one which adopts the optimum geometry for DABCO binding. The other isomer is distorted when it binds DABCO. We have not been able to determine whether it is the "syn" or "anti" isomer which accomodates DABCO best: molecular models give no clear indication of which isomer should bind in the optimum geometry.

**The Magnitude of the $\pi$–$\pi$ Interaction.** By using similar techniques to those in the following paper,[3] the thermodynamic data for DABCO–**Zn3** and DABCO–$Zn_21$ binding can be used to quantify the zinc porphyrin–zinc porphyrin $\pi$–$\pi$ interaction. The value of $\Delta S$ for DABCO binding to $Zn_21$ is similar to the value for binding to **Zn3**. The reason is that the $Zn_21$–DABCO complex is highly ordered, as revealed by its $^1$H NMR spectrum, but the free dimer also has a highly defined structure so that the conformational change on DABCO binding is associated with only a small entropy change. $\Delta S$ simply reflects the stoichiometry of the reactions. $\Delta H$, in contrast, differs for the two reactions: on binding to the dimer, DABCO forms two zinc–nitrogen bonds, whereas binding to the monomer involves only one zinc–nitrogen bond. Thus we might expect $\Delta H$ for binding to the dimer to be approximately twice that for binding to the monomer, but it is less than this because binding inside $Zn_21$ requires disruption of the porphyrin $\pi$–$\pi$ interaction. Taking the cooperativity in the second binding constant of DABCO into account, and assuming that the DABCO complex is strain free, as the NMR data suggest, we can estimate the energy of the zinc porphyrin $\pi$–$\pi$ interaction ($\Delta H_{\pi\pi}$):

$$\Delta H_{\pi\pi} = 2\Delta H(\text{Zn3–4}) - \Delta H(\text{Zn}_2\text{1–4}) + RT \ln \alpha = -48 \pm 10 \text{ kJ mol}^{-1}$$

$\Delta H$ is at the upper limit of previous widely varying estimates of the porphyrin-porphyrin interaction.[15] This approach for measuring intramolecular interactions will be discussed in more detail in the following paper, where we introduce the quantities $\Delta\Delta H$ and $\Delta\Delta S$ and extend the same experimental approach to dimers that enclose much larger cavities and afford additional $\pi-\pi$ interactions.[3]

A similar treatment is not possible for the $\pi-\pi$ interaction in $Zn_2$**2** because the formation of this complex is likely to be associated with an unfavorable strain energy, but we can make an estimate from the kinetic data. Binding by DABCO on the outside of $Zn_2$**2** cannot lead directly to a complex with DABCO bound inside the cavity. The first and rate-determining step is opening of the cavity (Figure 11). Only then can DABCO bind. Thus the activation energy for this process is the energy required to prise the two porphyrins apart which we estimated above to be 47-51 kJ mol$^{-1}$. There may be an entropy difference between the closed and open forms and some strain energy may be associated with the open form, so 47 kJ mol$^{-1}$ (11 kcal mol$^{-1}$) sets an upper limit on the $\pi-\pi$ interaction in this dimer.

We can now rationalize the exchange phenomena observed in the $^1$H NMR spectrum of free $Zn_2$**1**. An activation energy of 48 kJ mol$^{-1}$ would lead to fast exchange on the $^1$H NMR time scale at room temperature, and so the meso and racemic forms of $Zn_2$**1** would appear as an averaged set of signals at room temperature. We do indeed observe fast exchange at room temperature, with an estimated activation energy of 49 kJ mol$^{-1}$ (see above). There may be some entropic and possibly strain contribution to this energy, but, assuming that the major contribution is the $\pi-\pi$ interaction between porphyrins, this agrees with the calculated value of $\Delta H_{\pi\pi}$.

The kinetics of $Zn_2$**1**-DABCO binding indicate that binding of DABCO on the outside of the dimer reduces the strength of the $\pi-\pi$ interaction by at least 8 kJ mol$^{-1}$ (Figure 8), in agreement with previous studies on metalloporphyrin disaggregation by ligands.[6] Pyridine binding to a porphyrin dimer in which there is a strong $\pi-\pi$ interaction reduces the magnitude of the interaction and there is a concomitant reduction in the ligand binding energy relative to binding to a porphyrin monomer. The first binding energy of pyridine to the dimers, $Zn_2$**1** and $Zn_2$**2**, is reduced by 10 kJ mol$^{-1}$ relative to the energy for binding to **Zn3** (Table II), and we equate this loss in binding energy with a lowering of the porphyrin-porphyrin $\pi-\pi$ interaction. This agrees with our observations for DABCO binding.

## Conclusion

We have shown that DABCO can be used to generate a new series of supramolecular porphyrin complexes with defined geometries. The dimers $Zn_2$**1** and $Zn_2$**2** show diverse binding properties as a consequence of minor changes in structure, allowing us to probe subtly both the size of the binding pockets and the binding processes. The large variation in behavior we observe such as small two-component systems shows how the high selectivity which occurs in the binding and catalytic properties of multicomponent systems such as enzymes can arise.

We have also used these systems to measure the magnitude of the $\pi-\pi$ interaction between two zinc porphyrins and have investigated the disaggregation effects of ligand coordination on a quantitative level. These measurements along with our previous determination of the geometry of $\pi-\pi$ interactions will enable us to test theoretical models for this poorly understood phenomenon.[4]

**Acknowledgment.** We thank the DENI (C.A.H.) and SERC (M.N.M. and J.K.M.S.) for financial support.

# Thermodynamics of Induced-Fit Binding Inside Polymacrocyclic Porphyrin Hosts

**Harry L. Anderson, Christopher A. Hunter, M. Nafees Meah, and Jeremy K. M. Sanders***

*Contribution from the Cambridge Center for Molecular Recognition, University Chemical Laboratory, Lensfield Road, Cambridge CB2 1EW, U.K.* *Received October 31, 1989*

**Abstract:** The binding of bis-amine ligands to a series of cyclic zinc porphyrin dimers has been characterized by NMR and electronic spectroscopy. The cavity within the flexible dimers is kept closed by $\pi-\pi$ interactions between the porphyrin and aromatic bridging groups but can be opened by ligands whose binding is strong enough to overcome this energetic barrier. Analysis of the binding of these bifunctional and the corresponding monofunctional ligands to the porphyrin dimers and corresponding monomeric porphyrins allowed definition of the parameters $\Delta\Delta G$, $\Delta\Delta H$, and $\Delta\Delta S$. These are specifically associated with the energetic costs of conformational switching and yield information about the strength of the $\pi-\pi$ interactions that hold the cavity closed. It is estimated that the porphyrin-pyromellitimide $\pi-\pi$ interaction has an energy of 28-56 kJ mol$^{-1}$ (7-13 kcal mol$^{-1}$), while the porphyrin-biphenyl interaction is ca. 22 kJ mol$^{-1}$ (5 kcal mol$^{-1}$). A bis-pyridyl porphyrin ligand which has additional recognition sites binds within the cavity with no thermodynamic barrier. It is shown that similar values of $\Delta\Delta G$ can mask radically different binding modes: the values $\Delta\Delta H$ and $\Delta\Delta S$ are more informative, allowing the dissection of the various factors that contribute to or inhibit ligand binding within a cavity.

In the preceding paper[1] we showed how binding studies on the cofacial porphyrin dimers, **1** and **2**, allowed us to measure the $\pi-\pi$ interaction between two porphyrins; we now apply the same techniques to the larger flexible dimeric porphyrin macrocycles, **8**, **9**, and **10**,[2-4] with a view to understanding the more complex intramolecular interactions that control their conformational and binding properties. The relative conformations adopted by the aromatic components of these systems are as illustrated and are

(1) Hunter, C. A.; Meah, N. M.; Sanders, J. K. M., preceding paper in this issue.

(2) We continue the numbering scheme from the preceding paper.

(3) Preliminary communications: Hunter, C. A.; Meah, N. M.; Sanders, J. K. M. *J. Chem. Soc., Chem. Commun.* **1988**, 692-694 and 694-696.

(4) Leighton, P.; Sanders, J. K. M. *J. Chem. Soc., Perkin Trans. 1* **1987**, 2385-2393.

0002-7863/90/1512-5780$02.50/0 